

Evaluation of ^{86}Kr Cross Sections For Use in Fusion Diagnostics

M. Vorabbi,^{1,*} G.P.A. Nobre,^{1,†} D.A. Brown,¹ A.M. Lewis,^{2,‡} E. Rubino,^{3,§} and S. Mughabghab^{1,¶}

¹*National Nuclear Data Center, Brookhaven National Laboratory, Upton, NY 11973, USA*

²*Rensselaer Polytechnic Institute, Gaerttner LINAC Center, 110 8th Street, Troy, New York 12180*

³*Department of Physics, Florida Atlantic University, 777 Glades Road, Boca Raton, FL 33431, USA*

(Dated: January 30, 2022)

The National Ignition Facility at Lawrence Livermore National Laboratory uses ^{86}Kr as a diagnostic tool to measure the neutron flux produced by fusion reactions. As krypton is chemically inert, it can be implanted directly into the fuel capsule, and the reaction products can be measured to determine the flux of fusion neutrons. ^{86}Kr cross sections also provide model constraints for the ^{85}Kr branching point in the s-process and the neutron flux in stars. In this work, experimental data on the neutron production, radiative capture, inelastic scattering, and total cross sections of ^{86}Kr were used in conjunction with the fast region nuclear reaction code EMPIRE and a new resonance-region evaluation to produce a new evaluation of neutron-induced reactions on ^{86}Kr . For the EMPIRE calculations, we fitted the optical model potential up to 12 MeV to simultaneously reproduce the experimental data for the total cross section and the main inelastic gamma transition from the 2^+ state to the 0^+ ground state. This choice turned out to be very effective and produced a very good agreement of our calculations and the experimental data also for all the other inelastic transitions. For energies above 12 MeV, due to large fluctuations and uncertainties in the total cross section data, we preferred to adopt the Koning-Delaroche global spherical optical model potential. Always in this energy regime, the $(n, 2n)$ channel is dominant and the physics is dictated by the pre-equilibrium. In this energy regime we adopted the exciton model that was fitted to reproduce the available data in the $(n, 2n)$ channel and consistently produced a good description of the high-energy tail of the data for the inelastic gamma transitions. With these models and corrections to the structure of ^{86}Kr , the evaluated cross sections matched the experimental data. The new evaluation has been submitted for incorporation in the next release of the ENDF/B nuclear reaction library.

I. INTRODUCTION

The ^{86}Kr isotope is important in applications for both fusion technology and astrophysics. As a chemically inert noble gas, krypton can be frozen and implanted in the fuel capsules used at the National Ignition Facility (NIF) at Lawrence Livermore National Laboratory [1]. During a laser shot at NIF, the Kr nuclei are directly exposed to the neutron flux at the location of the burn, providing the most accurate picture of the fuel areal density. The RAGS (radiochemical analysis of gaseous samples) detector is then used to collect the krypton gas and analyze it for certain decay products that are produced by neutron-induced reactions with the fusion neutrons. The $^{86}\text{Kr}(n, 2n)^{85m}\text{Kr}$ and $^{86}\text{Kr}(n, \gamma)^{87}\text{Kr}$ reactions are of

particular interest for this application, as the resultant nuclei of both reactions de-excite with half-lives and energies that are convenient for measurement. The RAGS detector allows for the determination of the number of each isotope produced in the shot, which can be used to calculate the flux of neutrons caused by the fuel burn if the cross sections of the reactions are well understood.

The $^{86}\text{Kr}(n, 2n)^{85m}\text{Kr}$ and $^{86}\text{Kr}(n, \gamma)^{87}\text{Kr}$ reactions can also be useful as test cases in astrophysics. ^{85}Kr is an important branching point in the slow-neutron capture process (s-process) that occurs in asymptotic giant branch (AGB) stars, which are thought to produce about half of all elements heavier than iron [2]. Branching points in the s-process occur at isotopes with decay half-lives that are long enough to allow the neutron capture reaction to compete with the radioactive decay. In the case of ^{85}Kr , with a half-life of 10.75 y, neutron capture is competitive in typical AGB star environments, as shown in Fig. 1. Of course, the knowledge of the $^{85}\text{Kr}(n, \gamma)^{86}\text{Kr}$ cross section is extremely important to obtain information on the s-process from the study of this branching point, but, unfortunately, due to ^{85}Kr radioactivity, the $^{85}\text{Kr}(n, \gamma)^{86}\text{Kr}$ reaction has not been measured directly above thermal

* Primary author: mvorabbi@bnl.gov

† Corresponding author: gnobre@bnl.gov

‡ Current affiliation: Naval Nuclear Laboratory.

§ Current affiliation: National Superconducting Cyclotron Laboratory, Michigan State University.

¶ *In memoriam.*

- Change of resonance format from MLBW to RM in total cross sections.
- Setting the scattering radius R' to match the value recommended by the Atlas [15], that is 7.8 ± 0.1 fm.
- Adding the background artificial resonance at -20.0 keV (adopted from JENDL-4.0 [10]), but with tuned Γ_γ to set thermal capture cross section at the value of 3 mb. At first this may seem low, but it is worth noting that the 3 mb value is based solely on measurements of 4 primary gammas.
- Adding a missing resonance at 188.89 keV from Carlton *et al.* [11] using systematics for Γ_γ taken from JENDL-4.0 [10] (see Fig. 2).

Overall agreement of $^{86}\text{Kr}(n,\text{tot})$ improved dramatically at high energies on account of the format change, which can be clearly seen in Fig. 3; and at low energy mainly due to the new resonance (Fig. 2) and the change to R' . The $^{86}\text{Kr}(n,\gamma)$ cross section now goes through the thermal point, but is a bit lower than the average gamma data in experiment (Fig. 4). It is unclear, from the data perspective, whether this could be further improved. There were indications, however, that there may be missing p-wave resonances around the 188.89 keV resonance, as there seem to be small energy shifts in that region.

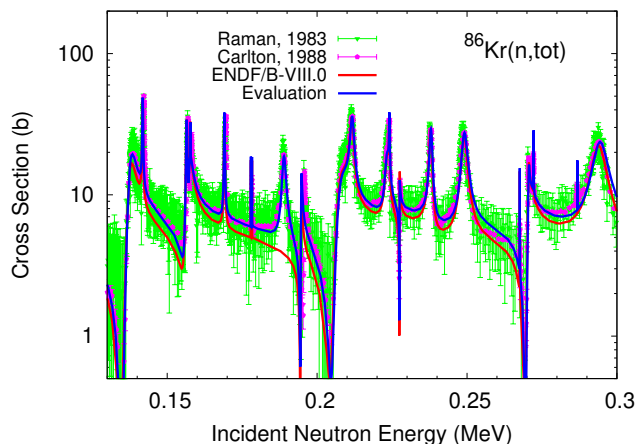


FIG. 2. Evaluation of the (n, tot) cross section. A missing resonance at 188.89 keV from Carlton *et al.* [11] has been added and the data background has also been corrected. Experimental data are taken from Refs. [11, 13].

In Table I the thermal cross-section values, the resonance integrals (RI), and the Maxwellian averaged cross section (MACS) of ^{86}Kr are reported for several evaluated and measured data. We note that the thermal values computed in this evaluation do not have uncertainties. A proper set of covariances in the thermal region and RRR would require a full R-matrix [23, 24] analysis, which is outside the scope of this work. The uncertainty

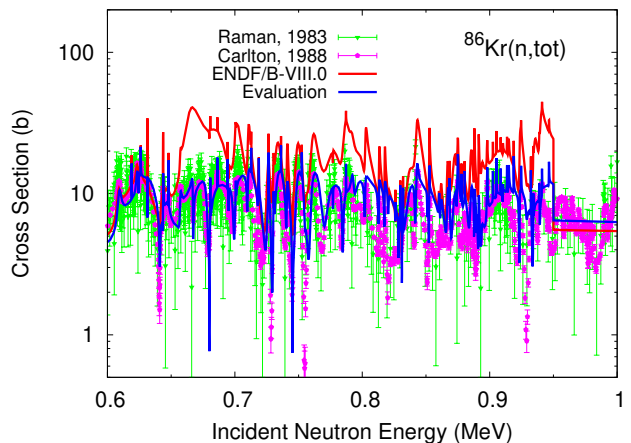


FIG. 3. Evaluation of the (n, tot) cross section for energies between 600 keV and 1 MeV. This significant improvement arises from the correct interpretation of the widths as Reich-Moore (RM) fits rather than Multi-level Breit-Wigner (MLBW). Experimental data are taken from Refs. [11, 13].

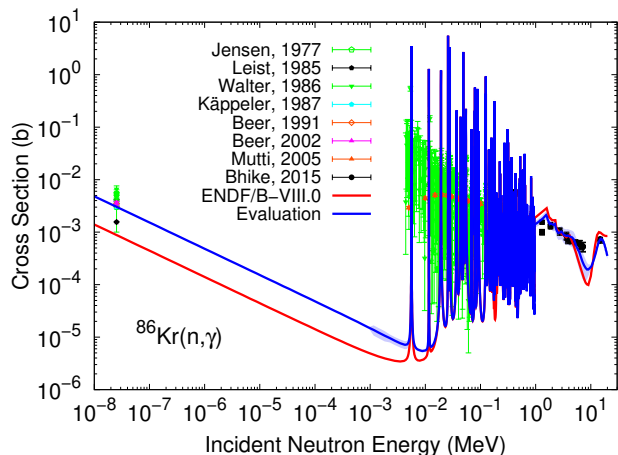


FIG. 4. Evaluation of the (n, γ) cross section compared to ENDF/B-VIII.0 [7]. Experimental data are taken from Refs. [5, 16–22].

bands seen in the cross-section plots in the RRR were obtained from extrapolated covariances from EMPIRE [6] calculations, which have energy lower-limit of ~ 1 keV, constrained by fast-region data¹.

III. EVALUATION IN THE FAST RANGE

In Section III A we discuss the experimental data in the fast range available to provide constraints on model calculations. These calculations are discussed in Section III B. The evaluated results are then presented in Section III C.

¹ See Section III C 1.

TABLE I. ^{86}Kr resonance region integral metrics. Atlas results marked with “exp” refer to the Mughabghab’s evaluation based on the experimental data, while Atlas values derived from calculations are marked with “calc”.

σ_{therm} (b)	(n,tot)	(n,el)	(n, γ)
This work ^a	6.695	6.689	3.028e-3
Atlas (2018) [15]	6.72 ± 0.37	6.72 ± 0.37	$(3 \pm 2)e-3$
ENDF/B-VIII.0 [7]	5.442	5.441	8.790e-4
JEFF-3.3 [25]	5.824	5.818	2.968e-3
JENDL-4.0 [10]	6.155	6.150	3.001e-3
RI (b)	(n,tot)	(n,el)	(n, γ)
This work	114.3 ± 1.4	109.6 ± 1.4	$(20.4 \pm 1.3)e-3$
Atlas (2018) [15]			$(18 \pm 2)e-3$
ENDF/B-VIII.0 [7]	100.5	97.35	20.00e-3
JEFF-3.3 [25]	110.7	104.3	18.70e-3
JENDL-4.0 [10]	105.1	101.2	23.42e-3
MACS(30 keV) (mb)	(n,tot)	(n,el)	(n, γ)
This work	7880 ± 310	7870 ± 310	5.08 ± 0.28
Atlas (exp) (2018) [15]			4.76 ± 0.28
Atlas (calc) (2018) [15]			5.3 ± 0.5
ENDF/B-VIII.0 [7]	6639	6634	5.063
JEFF-3.3 [25]	6977	6973	4.084
JENDL-4.0 [10]	7335	7330	5.112
Kadonis-1.0 ^b [26]			4.76 ± 0.28
Käppeler (2021) [27]			4.8 ± 0.7
Mutti (2005) [16]			4.76 ± 0.28
Beer (1991) [19]			3.34 ± 0.24
Walter (1986) [17]			5.6 ± 0.7
Walter (1986) [28]			3.8 ± 0.7
Raman (1983) [13]			4.8 ± 1.2

^a Thermal values do not have uncertainties since EMPIRE [6] can only generate covariances down to 1 MeV.

^b This value is taken from Ref. [16] where the authors used Xenon as a reference.

A. Availability of Experimental Data

In the fast region we have data for only four processes: total, inelastic γ -transitions, (n,2n), and radiative capture. The (n,2n) channel opens up at an energy of ~ 10 MeV and can be considered at a later stage during the evaluation. Also, the radiative capture cross section is much smaller compared to the cross section of the other processes, so it can be considered in a later step of the evaluation.

For the total cross section we have two data sets: one from Raman *et al.* [13], which covers the energy range that goes from 4 keV to 5 MeV, and another one measured by Carlton *et al.* [11] covering a wider energy range that goes from 1 MeV to 25 MeV. For this latter set, some considerations have to be made. Due to poor statistics, it provides different levels of reliability depending on the incident energy of the incoming neutron. In particular, in

the energy range between 1 and 8 MeV the average cross section has small error bars and thus can be trusted with a higher degree of confidence. In contrast, for higher energies the uncertainties become larger, but it is still possible to identify an intermediate range, from 8 to 12 MeV, where the average cross section has still relatively small error bars and the data can still be trusted. Above 12 MeV the uncertainties and fluctuations in the average cross section are too large and it is not possible to rely on the data anymore.

In addition to the (n,tot) data we also have precise data for 12 inelastic transitions [29] that we can use to constrain our model. With a simple look at the data one realizes that the cross sections for the different transitions are in general of the same order of magnitude except for two that are larger. In particular, the transition from the first excited state (2^+) to the ground state (0^+) is dominant with one order of magnitude of difference with respect to the second most important transition and almost two orders of magnitude with respect to all the other ones. Based on these considerations we adopted the following strategy: we performed two different fits of the (n,tot) data in the first two energy regions, *i.e.* from 0.5 to 8 MeV and from 8 to 12 MeV, and we fitted our optical potential to simultaneously reproduce these fits and the data of the $2^+ \rightarrow 0^+$ inelastic transition for energies up to 11 MeV. For energies above 12 MeV we adopted the pure Koning-Delaroche [30] optical potential and we performed a smooth transition between the fitted potential and the pure Koning-Delaroche potential in the energy region between 11 and 12 MeV. Finally, for energies above 12 MeV the description of the (n,2n) data should be dictated by the pre-equilibrium, so for this energy range we tuned the pre-equilibrium model to simultaneously reproduce the (n,2n) data and the high-energy inelastic data.

B. Reaction Model Parametrizations

We employed the EMPIRE nuclear reaction code [6] for model calculations and parameter tuning aiming to evaluate the reaction channels in the fast region (*i.e.*, neutron incident energies above the first inelastic excitation energy). The level-density (LD) model adopted was the combinatorial Hartree-Fock-Bogoliubov (HFB) from RIPL-3 [31], as its microscopic nature should in principle provide more realistic spin and parity distributions for a nucleus with such scarce availability of data such as ^{86}Kr . The lack of differential spectra data prevented us from using the approach of Ref. [32] to fine tune and better constrain the LD, as it has been done recently in Ref. [33]. We adjusted the LD to optimize the agreement with observed discrete levels. Fig. 5 shows the experimental discrete levels compared to the cumulative level distributions obtained from the adopted LD for the residual nuclei of the relevant reactions for the current evaluation. The continuum energy cut-off E_{cut} , above which levels are considered to be in the continuum and calculations switch

from discrete levels to LD, were 2.787, 4.070, 1.400, and 0.582 MeV for ^{87}Kr , ^{86}Kr , ^{85}Kr , and ^{83}Se , respectively, and are marked as dashed arrows in the plots. We can see that, generally, there is a very good agreement of the distribution and its shape with the discrete levels at and around E_{cut} .

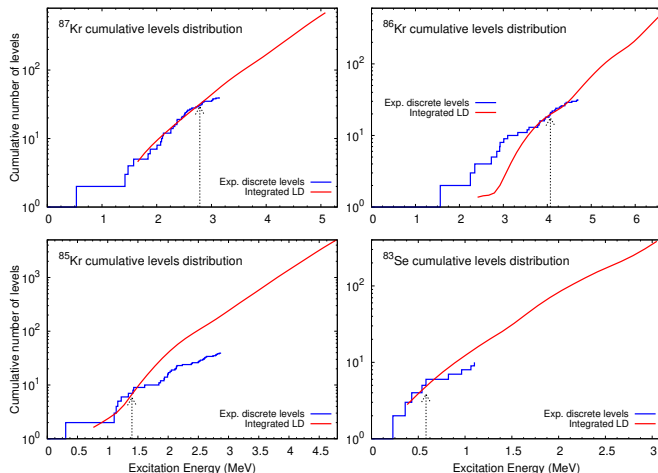


FIG. 5. Cumulative level distribution obtained from the levels listed in RIPL-3 [31] (blue lines) compared with the level densities employed (red curves) in our model calculations for the residual nuclei from the main reactions studied in this evaluation work. Dashed arrows show the discrete-level cutoff adopted indicating transition to level continuum.

Width fluctuation corrections were applied up to 9.0 MeV and pre-equilibrium was determined using the exciton model [34] as implemented in the code PCROSS [35], with mean free-path, single-particle LD parameter, and coefficient defining the equilibrium cross-section data. The complete γ -ray cascades were calculated and we assumed the RIPL-3 MLO1 formulation by Plujko for E1 transitions initiated from the continuum for the γ -strength functions of all residual nuclei produced [31, 36]. Electromagnetic transitions of multipolarity M1, E1 and E2 were considered. The decay from the compound nucleus was added incoherently to the direct cross sections. Blatt-Biedenharn coefficients were employed to calculate compound-nucleus anisotropy [37].

In Table II, we identify the optical model potentials (OMPs) employed for the different reaction channels. For the direct reaction component, due to the lack of recent local OMP specific to ^{86}Kr , we adopted the spherical OMP of Koning-Delaroche. One of the main experimental constraints for this evaluation are cross-section data from gamma transitions between inelastic levels, which is highly dependent on level-coupling mechanisms. Therefore, we opted to describe explicitly some of these couplings. For that, we employed coupled-channel calculations within a rigid rotational model, coupling to the first 2^+ and 4^+ states using a quadrupole deformation

of $\beta_2 = 0.145$ [31, 38] and the Koning-Delaroche as the bare potential. This allows for minor tuning of total and absorption cross sections following the data available. This corresponds to an intermediate approach between spherical nuclei and adiabatic approximations for more strongly-deformed nuclei [39], which is consistent with the intermediate deformation seen in ^{86}Kr . Levels computed in the distorted-wave Born approximation (DWBA) were considered in calculations up to the transition to continuum at 4.07 MeV in order to improve agreement with inelastic gamma data and to generate neutron production spectra without gaps in the transition to continuum/preequilibrium contributions.

TABLE II. Optical model potentials used in the EMPIRE [6] calculations. The “CC” label indicates a coupled-channels optical model potential, in contrast with the spherical ones.

Ejectile	Type	RIPL #	Reference
n (direct)	CC	2405	Koning+ [30]
	(rotational model)		
n (compound)	Spher.	2405	Koning+ [30]
p	Spher.	5405	Koning+ [30]
α	Spher.	9600	Avrigneanu+ [40]
d	Spher.	6200	Haixia+ [41]
t	Spher.	7100	Becchetti+ [42]
^3He	Spher.	8100	Becchetti+ [42]

C. Results

We present here the main results for the current evaluation. Whenever data is not shown, it can be assumed there are no experimental data available in the literature for that particular reaction and/or energy range. Experimental data, when present, were obtained through the experimental nuclear reaction data (EXFOR) [43, 44] web utility.

1. Covariances

The lack of sufficient experimental data and detailed documentation of uncertainty sources prevented us from developing a more quantitative, higher fidelity set of covariances matrices. For this reason we provide lower-fidelity covariances in the fast region obtained through model parameter variations using the KALMAN code [45]. This was done by tuning the weight of experimental constraints until the uncertainties for each reaction were qualitatively compatible with the expected cross-section uncertainties that can be inferred from the actual data. We extended these covariances down to 1 keV.

2. Total Cross Section

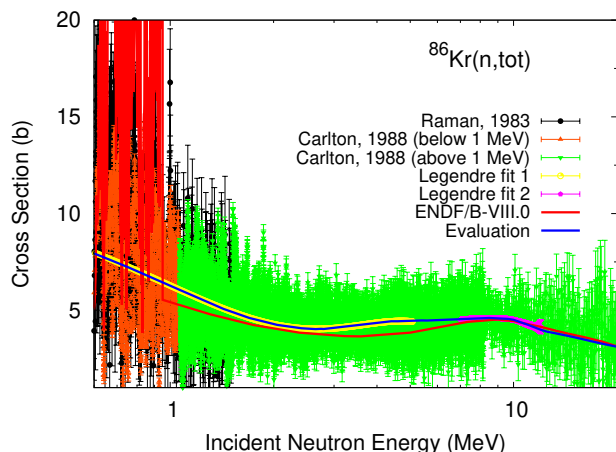


FIG. 6. Evaluation of the (n, tot) cross section computed with EMPIRE [6] and compared with the two fits of the experimental data. Due to different statistics we performed two different fits of the data for two energy regions 0.5-8 MeV and 8-12 MeV. Experimental data are taken from Refs. [11, 13]. Ref. [11] reports different averages for data below and above 1 MeV, and in this work we maintained this distinction.

Two measurements of the total cross section of ^{86}Kr were performed by transmission at ORELA. In 1983 Raman *et al.* measured the total cross section in the energy region between 4 keV and 5 MeV [13], and in 1988, Carlton *et al.* measured the cross section in the energy region between 1 MeV and 25 MeV [11]. The experimental data were energy averaged because of the overwhelming number of data points, to provide a more appropriate comparison with the calculated cross sections². In Fig. 6 we display the EMPIRE [6] calculation of the total cross section compared with the two fits (yellow and purple lines) of the experimental data that are very nicely reproduced. The same calculation is also presented in Fig. 7 along with the resonances and the uncertainty band of the total cross section obtained from the covariance matrix.

3. Inelastic Scattering Cross Sections

The inelastic scattering reaction provides valuable insight into the nuclear structure of the target nucleus. The compound nucleus decays by emission of a neutron, leaving an excited ^{86}Kr nucleus that de-excites by gamma emission. The inelastic scattering gammas are the energy given off as the nucleus transitions from one level

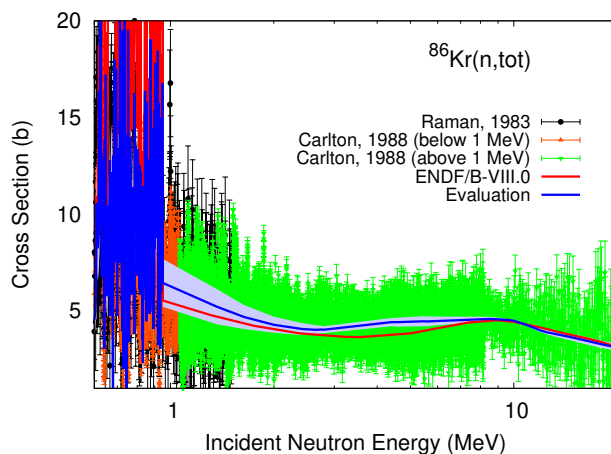


FIG. 7. Evaluation of the (n, tot) cross section computed with EMPIRE [6] and compared with the experimental data [11, 13]. The light-blue band represents the uncertainty band obtained from the covariance matrix. Ref. [11] reports different averages for data below and above 1 MeV, and in this work we maintained this distinction.

to another, and therefore can be used to study the nuclear structure. Partial gamma cross sections for thirteen such transitions were measured by Fotiadis *et al.* [29] for incident neutron energies up to 20 MeV.

The $^{86}\text{Kr}(n, n'\gamma)^{86}\text{Kr}$ experiment was conducted at the Los Alamos Neutron Science Center (LANSCE) facility using the Germanium Array for Neutron Induced Excitations (GEANIE) detector system. GEANIE consists of 10 Compton-suppressed planar Germanium detectors and 10 Compton-suppressed coaxial Germanium detectors, but the results of the experiment only come from 4 of the latter detectors chosen for optimal time and energy resolution. The neutron flux was measured using a fission chamber containing ^{238}U and ^{235}U foils. There were ten new transitions discovered that had not previously been observed for this reaction and overall, they measured partial cross sections for 22 transitions at neutron energies between 1 MeV and 20 MeV. The neutron beam was pulsed and the experimenters used the time-of-flight method to determine the incident energy of the neutrons on target. The experimenters used natural iron foils on either side of krypton cell, perpendicular to the beam, so the known cross section at 14.5 MeV incident energy of the $846\text{ keV } 2^+ \rightarrow 0^+$ could be used for normalization of the cross sections in the krypton experiment. The experimenters also accounted for the efficiency of the detectors, target thickness, and “dead-time” of the neutron beam. More experimental details can be found in Ref. [29].

In an effort to properly reproduce the partial gamma cross section we had to provide branching ratios and γ -ray energies for several levels that contained incomplete or uncertain structure data. Without these corrections, there would be ambiguity in the decay and EMPIRE [6] would assume that the levels in question decay straight

² The computed optical model and Hauser-Feshbach cross sections are energy averages of the fluctuating compound nuclear cross sections.

to the ground state. Thus, it was necessary to determine the possible γ -rays, multipolarities, spins, parities, and branching ratios for each energy level with unspecified decay data in ^{86}Kr using selection rules and systematics. In Table III we display all the discrete levels with uncertain J^π assignment and the adopted values that we used to perform our calculations. Similarly, in Table IV we display all the γ -rays that we introduced to avoid direct transitions to the ground state. It is worth notice that in this work we adopted the convention of representing the ground state with the level index 1, the first excited state with the index 2, and so forth.

TABLE III. Adopted J^π values for discrete levels of ^{86}Kr . In this work we adopted the convention of representing the ground state with the index 1, the first excited state with the index 2, and so forth. All the energies are in MeV.

Level	E	ENSDF J^π	Adopted J^π
6	2.85072	(2, 3) ⁺	2 ⁺
7	2.91683	(3) ⁻	3 ⁺
9	3.00943	(1, 2) ⁺	2 ⁺
11	3.32810	(3 ⁺ , 4 ⁺)	4 ⁺
13	3.58340	(0 ⁺ to 4 ⁺)	4 ⁺
15	3.81632	(5 ⁺)	5 ⁺
17	3.93530	(5)	5 ⁺
18	3.95900	(3 ⁻ , 4 ⁺)	4 ⁺
19	4.03860	(2, 3) ⁻	3 ⁻
20	4.06412	(6 ⁺)	6 ⁺

TABLE IV. New γ -rays introduced. In this work we adopted the convention of representing the ground state with the index 1, the first excited state with the index 2, and so forth. All the energies are in MeV. The subscript i stands for “initial” while f stands for “final”. The last column shows the branching ratios that we assumed for these transitions.

Level _{i}	E_i	J_i^π	E_γ	Level _{f}	E_f	J_f^π	BR
11	3.3281	4 ⁺	1.078	3	2.25001	4 ⁺	0.4
16	3.8320	0 ⁺	0.823	9	3.00943	2 ⁺	0.4828
16	3.8320	0 ⁺	1.483	4	2.34947	2 ⁺	0.05823
16	3.8320	0 ⁺	2.267	2	1.56461	2 ⁺	0.4589
18	3.9590	4 ⁺	0.631	11	3.32810	4 ⁺	0.04030
18	3.9590	4 ⁺	0.860	10	3.09885	3 ⁻	0.01197
18	3.9590	4 ⁺	1.042	7	2.91683	3 ⁺	0.02061
18	3.9590	4 ⁺	1.610	4	2.34947	2 ⁺	0.01579
18	3.9590	4 ⁺	1.709	3	2.25001	4 ⁺	0.8018
18	3.9590	4 ⁺	2.394	2	1.56461	2 ⁺	0.1095

For some levels used in our calculations, a specific J^π assignment was not given in the Evaluated Nuclear Structure Data Files [46, 47] (ENSDF) and a range of possible assignments was given. For some of these levels it was possible to provide a unique J^π assignment using the values provided in Table IV of Ref. [48], which reports the results of a subsequent measurement performed after the ENSDF evaluation where some of these J^π assignments

were better constrained through angular correlation measurements. We also used the information contained in Ref. [48] to improve our transition scheme with the addition of new transitions not included in ENSDF. Despite that, we still had to provide unique J^π quantum numbers for some levels. This is the case of levels 9, 11, and 13. The ENSDF J^π assignments are determined based on radioactive decay, inelastic scattering measurements, stripping reactions and known gamma transitions. For these three levels there was no conclusive choice given, and so in the original EMPIRE [6] run, we selected the higher-spin option. For level 7, a single J^π assignment was given in ENSDF, but experiments had suggested other possibilities as well. The J^π assignments for these four levels were changed based on patterns in the energy dependence of the experimental data, and for each level a new assignment was found which produced calculated cross sections with energy dependencies that fit the experimental data. For level 11, the change in spin opened up a new M1 gamma transition of comparable strength with the known transition, and so the branching ratio for this decay route was calculated using the Weisskopf single-particle estimates [49] and systematics for the average B(E1), B(E2), and B(M1) for isotones with N=50 [50]. The mean values of B(E1), B(E2) and B(M1) were found to be 6.823 ± 1.450 , $9.398 \times 10^{-7} \pm 2.534 \times 10^{-4}$, and 0.2046 ± 0.1442 respectively. For all the other levels we used the assignments provided by RIPL without any change.

In Fig. 8 we display the comparison between the data and our evaluation for the first inelastic transition while all the other ones are shown in Fig. 9. In this case there is no comparison with ENDF/B-VIII.0 [7] because any γ -ray production information is currently provided in the library. As for the case of the total cross section, the remarkable agreement between our calculation and the data for the $2^+ \rightarrow 0^+$ transition is not surprising since it is the result of a fit of the optical potential for energies up to 12 MeV and the pre-equilibrium model for higher energies. On the contrary, it is interesting to notice how the fit of the optical potential and the pre-equilibrium model were able to produce results for all the other transitions that are overall in good agreement with the data. In particular, it is worth noting how the data for the $4^+ \rightarrow 2^+$ transition, showed in the top left panel of Fig. 9, is remarkably well reproduced.

4. Neutron Production Cross Section

The $^{86}\text{Kr}(n, 2n)^{85m}\text{Kr}$ reaction is important for both the NIF diagnostics and for understanding the ^{85}Kr branching point in the s-process. The first excited state of ^{85}Kr is an isomer, and the decay of this isomeric state also provides a convenient method to measure the total (n, 2n) reaction rate in RAGS detector, providing information on the primary fusion neutrons. Two sets of experimental data are available for the $^{86}\text{Kr}(n, 2n)^{85m}\text{Kr}$ isomer reaction. One set was measured at the Triangle

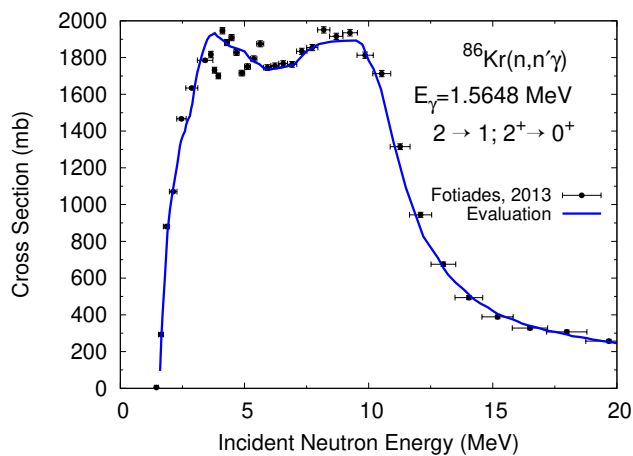


FIG. 8. Evaluation of the inelastic gamma cross section for the discrete transition from the 2^+ state to the 0^+ state. The indices for initial and final levels of the transition, with their corresponding spin and parity, as well as the γ energy, E_γ , are listed in the plot. In this work we adopted the convention of representing the ground state with the index 1, the first excited state with the index 2, and so forth. Experimental data are taken from Ref. [29]. We do not show ENDF/B-VIII.0 here as inelastic gamma information was not present in that evaluation.

Universities Nuclear Laboratory (TUNL) by Bhike *et al.* [5], in the energy range between 10 MeV and 15 MeV. A single measurement of the $^{86}\text{Kr}(n, 2n)^{85m}\text{Kr}$ cross section was taken by Kondaiah *et al.* [51], at the Georgia Tech accelerator at 14.4 MeV. Fig. 10 presents the experimental data for the isomer reaction, along with the evaluated cross section, which was calculated with EMPIRE [6] tuning the exciton model to reproduce the shape of the data of Bhike *et al.* We favored that experiment as it is much more recent and complete than the one from Kondaiah *et al.*

5. Radiative Capture Cross Section

The $^{86}\text{Kr}(n, \gamma)^{87}\text{Kr}$ reaction is important for studying the low energy component of the NIF flux, and for calculating the abundance of ^{87}Kr in AGB stars. Bhike *et al.* [5] measured the radiative capture cross section in the energy region between 0.5 MeV and 15 MeV in 2015. This set of experimental data is presented in Fig. 11, along with the calculated and evaluated cross section that is also compared with ENDF/B-VIII.0 [7]. We also display in light blue the uncertainty band obtained from the covariance matrix.

6. Partial Alpha Production Cross Section

For this case we only have one data point from Kondaiah *et al.* [51] for the $^{86}\text{Kr}(n, \alpha)^{83g}\text{Se}$ process. Since no

other information is currently available we tuned the α production mechanism to reproduce this data. Our evaluated cross section for this process is displayed in Fig. 12 along with the cross section for the isomeric state and their sum. It is worth notice that there is a significant difference between our results and ENDF/B-VIII.0 [7], because the latter does not include any isomeric cross section and the result displayed in red in Fig. 12 represents the total cross section, that was fitted to reproduce the only available point for the $^{86}\text{Kr}(n, \alpha)^{83g}\text{Se}$ process.

7. Neutron Emission Spectra

In general, there are several measurements of neutron energy spectra concentrated around 14 MeV for many nuclei. At these incident energies, the high outgoing-energy end of the spectra is dominated by the elastic peak and direct transitions to the collective levels that are well modeled by CC and DWBA calculations. The middle part of the spectrum is governed by the pre-equilibrium emission, while the low energy peak is the evaporation peak described by the Hauser-Feshbach model. Proper description of the neutron spectra is thus a very good overall test of the quality of the reaction modeling used in the evaluation.

Energy-angle correlated cross sections add another dimension to the energy spectra, associated with the scattering angle. These arguably correspond to an even more direct kind of measurement since energy spectra are usually obtained by integrating double-differential ones which unavoidably involves some approximations related to interpolation and extrapolation of angular distributions. However, employed models in EMPIRE [6] rely on empirical Kalbach parameterization of double-differential cross sections [52]. Therefore, comparison of an evaluation with double-differential cross sections provides for an additional stringent test of the modeling employed in the evaluation procedure.

Unfortunately, in the specific case of ^{86}Kr there are no spectra data available to guide our model parametrization. However, a direct comparison of our evaluation with ENDF/B-VIII.0 [7], as seen in Fig. 13 for different scattering angles and values of incident energy, shows that our careful description of inelastic couplings and pre-equilibrium provides a much more realistic spectra, without the gaps seen in ENDF/B-VIII.0. Therefore, our evaluation represents a major improvement in the the description of the inelastic process.

IV. CONCLUSIONS

A new ^{86}Kr evaluation was performed based on a new resolved resonance region evaluation and several sets of experimental data. The calculation of the neutron-induced reactions was performed using an optical model potential properly fitted to reproduce the experimental

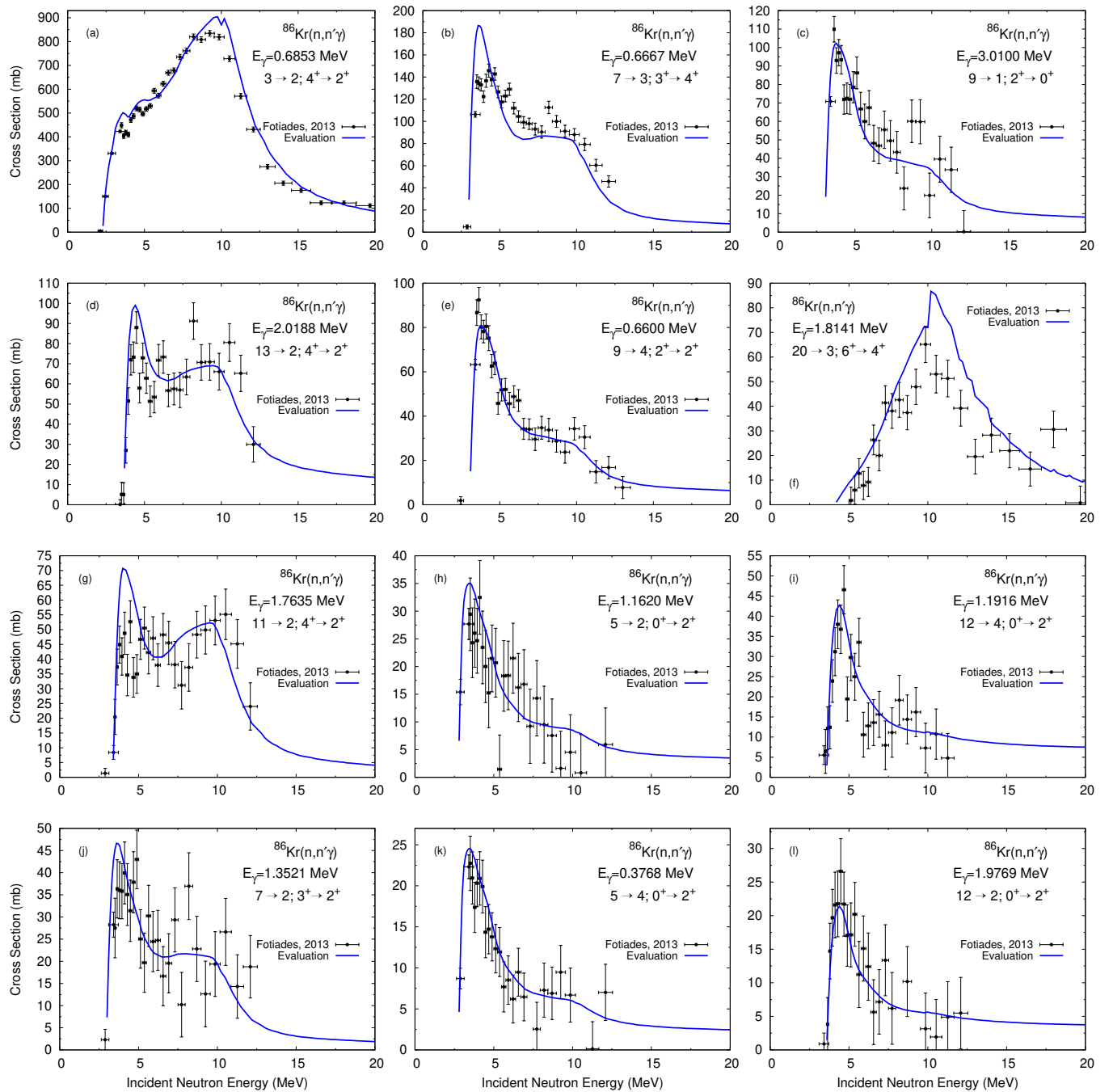


FIG. 9. Inelastic gamma cross sections for discrete transitions between excited levels of ^{86}Kr . The indices for initial and final levels of the transitions, with their corresponding spin and parity, as well as the γ energies, E_γ , are listed in the plots. In this work we adopted the convention of representing the ground state with the index 1, the first excited state with the index 2, and so forth. Our evaluation (blue curves) is compared to the experimental data measured by Fotiades *et al.* [29] (black points). We do not show ENDF/B-VIII.0 here as inelastic gamma information was not present in that evaluation.

data for the total cross section and the main inelastic gamma transition $2^+ \rightarrow 0^+$ for energies up to 12 MeV. Due to poor statistics and the consequent large fluctuations in the data for the total cross section, the Koning-Delaroche optical model potential was adopted at higher energies along with the exciton model that was properly

tuned to reproduce the $(n, 2n)$ experimental data. Several level J^π assignments and branching ratios were also fixed in the ^{86}Kr structure, leading to an overall evaluation that fits the experimental data. The accurate evaluation of the neutron production and radiative capture reactions will improve the modeling and calculations for the RAGS

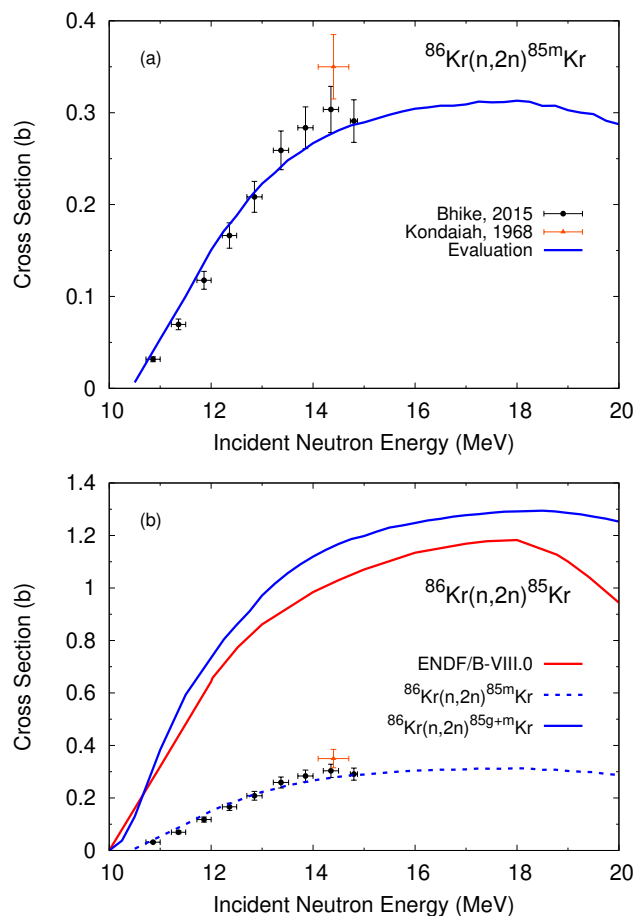


FIG. 10. Panel (a): evaluation of the $(n, 2n)$ isomer cross section. Two sets of experimental data [5, 51] are presented along with the evaluated cross section. Panel (b): Comparison of the evaluated total $(n, 2n)$ cross section with ENDF/B-VIII.0. No experimental data are available for this observable. For reference, the isomeric cross section and data from panel (a) are also shown.

detector at NIF and understanding of the ^{85}Kr branching point in the s-process. The new inelastic partial gamma evaluation provides insight into the nuclear structure of ^{86}Kr and may be used in future structure evaluations.

The evaluation presented here is a major improvement when compared to the previous ENDF/B-VIII.0 [7] file as it not only reproduces new measured data in detail but also corrects issues with thermal capture and total cross sections in the RRR, as well as provides data-constrained inelastic γ production and isomeric cross sections. Inelastic spectra are also much more realistic even though the lack of data prevented us to describe it in more detail. This new evaluation of the neutron-induced reactions on ^{86}Kr provides for the first time recommended values for γ -ray production, extremely important for the NIF diagnostics, and isomeric cross section production, and it has been submitted to be considered for inclusion in the next release of the ENDF/B library.

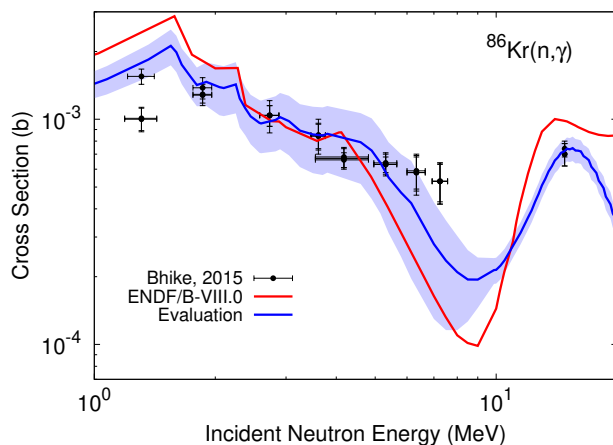


FIG. 11. Evaluation of the (n, γ) cross section compared with ENDF/B-VIII.0 [7] and the experimental data [5]. The light-blue band represents the uncertainty band of the cross section and it is obtained from the covariance matrix.

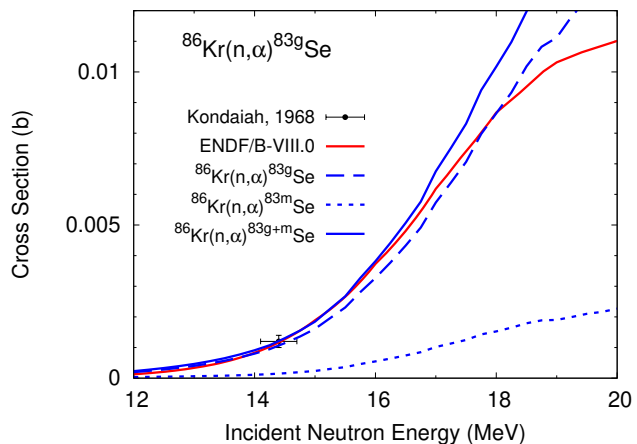


FIG. 12. Evaluation of the (n, α) cross section compared with the only available data taken from Ref. [51], which corresponds to the residual nucleus ^{83}Se in the ground state. Since no other information is available, we tune the alpha production mechanism to reproduce this data.

ACKNOWLEDGMENTS

Work at Brookhaven National Laboratory was sponsored by the Office of Nuclear Physics, Office of Science of the U.S. Department of Energy under Contract No. DE-SC0012704 with Brookhaven Science Associates, LLC. This project was supported in part by the U.S. Department of Energy, Office of Science, Office of Workforce Development for Teachers and Scientists (WDTS) under the Science Undergraduate Laboratory Internships Program (SULI). We would like to thank Dr. Balraj Singh, Dr. Alexandru Negret, and Dr. Elizabeth McCutchan for elucidative discussions on nuclear structure and level-spin assignments.

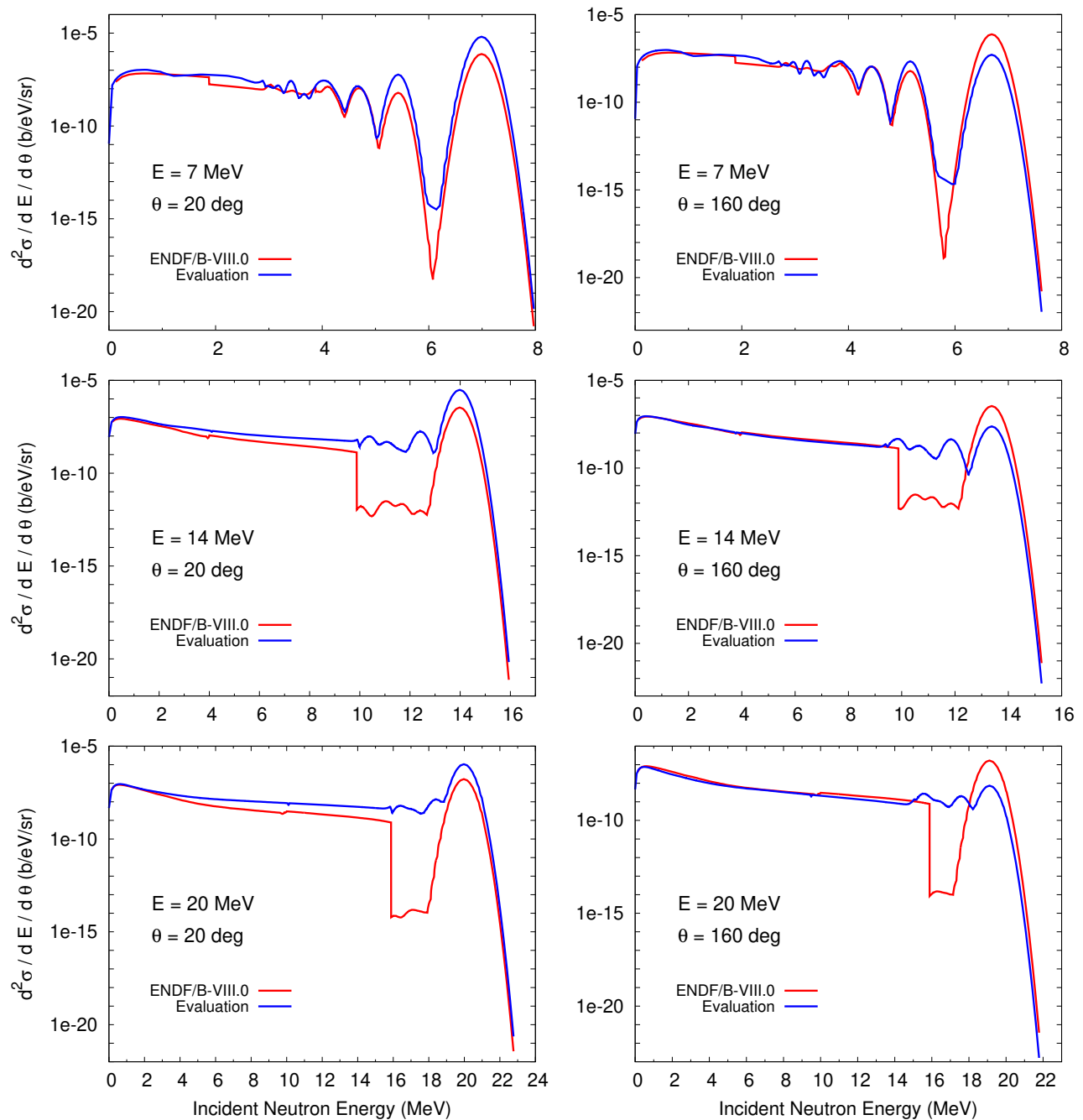


FIG. 13. Double differential cross sections computed at different incident energies and scattering angles compared with ENDF/B-VIII.0 [7].

-
- [1] A. Heller, “A new detector for analyzing NIF experiments,” *SCI. TECHNOL. REV.* (2012).
- [2] R. Raut, A. P. Tonchev, G. Rusev, *et al.*, “Cross-section measurements of the $^{86}\text{Kr}(\gamma, n)$ reaction to probe the s -process branching at ^{85}Kr ,” *PHYS. REV. LETT.* **111**, 112501 (2013).
- [3] C. E. B. Jr., R. E. Druschel, J. Halperin, and J. R. Walton, “Thermal-neutron capture cross section and resonance integral for 10.7-year krypton-85,” *NUCL. SCI. ENG.* **47**, 371 (1972).
- [4] R. Schwengner, R. Massarczyk, G. Rusev, *et al.*, “Pygmy dipole strength in ^{86}Kr and systematics of $n = 50$ isotones,” *PHYS. REV. C* **87**, 024306 (2013).

- [5] M. Bhide, E. Rubino, M. E. Gooden, Krishichayan, and W. Tornow, “Measurements of the $^{86}\text{Kr}(n, \gamma)^{87}\text{Kr}$ and $^{86}\text{Kr}(n, 2n)^{85}\text{Kr}^m$ reaction cross sections below $E_n = 15$ MeV,” *PHYS. REV. C* **92**, 014624 (2015).
- [6] M. Herman, R. Capote, B. V. Carlson, P. Obložinský, M. Sin, A. Trkov, H. Wienke, and V. Zerkin, “EMPIRE: Nuclear reaction model code system for data evaluation,” *NUCL. DATA SHEETS* **108**, 2655 (2007).
- [7] D. Brown, M. Chadwick, R. Capote, *et al.*, “ENDF/B-VIII.0: The 8th major release of the nuclear reaction data library with CIELO-project cross sections, new standards and thermal scattering data,” *NUCL. DATA SHEETS* **148**, 1 (2018).
- [8] M. B. Chadwick, M. Herman, P. Obložinský, *et al.*, “ENDF/B-VII.1 nuclear data for science and technology: Cross sections, covariances, fission product yields and decay data,” *NUCL. DATA SHEETS* **112**, 2887 (2011).
- [9] S. F. Mughabghab, *Atlas of Neutron Resonances, 5ed., Resonance Parameters and Thermal Cross Sections, Z = 1-100*. Elsevier, Amsterdam (2006).
- [10] K. Shibata, O. Iwamoto, T. Nakagawa, *et al.*, “JENDL-4.0: A new library for nuclear science and engineering,” *J. NUCL. SCI. TECHNOL.* **48**, 1 (2011).
- [11] R. F. Carlton, R. R. Winters, C. H. Johnson, N. W. Hill, and J. A. Harvey, “Total cross section and resonance spectroscopy for $n+^{86}\text{Kr}$,” *PHYS. REV. C* **38**, 1605 (1988).
- [12] S. F. Mughabghab, M. Divadeenam, and N. E. Holden, *Neutron Cross Sections, Vol.1, Neutron Resonance Parameters and Thermal Cross Sections, Part A, Z = 1-60*. Academic Press, New York (1981).
- [13] S. Raman, B. Fogelberg, J. A. Harvey, R. L. Macklin, P. H. Stelson, A. Schröder, and K. L. Kratz, “Overlapping β decay and resonance neutron spectroscopy of levels in ^{87}Kr ,” *PHYS. REV. C* **28**, 602 (1983).
- [14] P. Obložinský, ed., *Evaluated Data Library for the Bulk of Fission Products, Subgroup 23*. Paris: Nuclear Energy Agency, OECD (2009).
- [15] S. F. Mughabghab, *Atlas of Neutron Resonances, Vol.1 and 2*. Elsevier, Amsterdam (2018).
- [16] P. Mutti, H. Beer, A. Brusegan, F. Corvi, and R. Gallino, “New Kr Cross Sections and Astrophysical Constraints on Presolar Grains,” *AIP CONF. PROC.* **769**, 1327 (2005).
- [17] G. Walter, B. Leugers, F. Käppeler, Z. Y. Bao, G. Reffo, and F. Fabbri, “Kilo-electron-volt neutron capture cross sections of the krypton isotopes,” *NUCL. SCI. ENG.* **93**, 357 (1986).
- [18] F. Käppeler, A. A. Naqvi, and M. Al-Ohali, “Stellar krypton cross sections at $kT=25$ and 52 keV,” *PHYS. REV. C* **35**, 936 (1987).
- [19] H. Beer, “Capture Cross Section Measurements of Krypton and Xenon Isotopes and the Fundamental Parameters of the s-Process,” *AP. J.* **375**, 823 (1991).
- [20] H. Beer, P. Sedyshev, W. Rochow, P. Mohr, and H. Oberhammer, “Neutron capture measurements of the noble gas isotopes ^{22}Ne , ^{40}Ar and $^{78,80,84,86}\text{Kr}$ in the keV energy region,” *NUCL. PHYS. A* **705**, 239 (2002).
- [21] B. Leist, W. Ziegert, M. Wiescher, K. L. Kratz, and F. K. Thielemann, “Neutron capture cross sections for neutron-rich isotopes,” *Z. FÜR PHYSIK A* **322**, 531 (1985).
- [22] C. M. Jensen, R. G. Lanier, G. L. Struble, L. G. Mann, and S. G. Prussin, “Gamma rays from thermal neutron capture in ^{86}Kr ,” *PHYS. REV. C* **15**, 1972 (1977).
- [23] A. M. Lane and R. G. Thomas, “R-matrix theory of nuclear reactions,” *REV. MOD. PHYS.* **30**, 257 (1958).
- [24] G. Breit, *Theory of Resonance Reactions and Allied Topics*, 1. Berlin, Heidelberg: Springer Berlin Heidelberg (1959).
- [25] A. J. M. Plompen, O. Cabellos, C. De Saint Jean, *et al.*, “The Joint Evaluated Fission and Fusion nuclear data library, JEFF-3.3,” *THE EUR. PHYS. J. A* **56**, 181 (2020).
- [26] “KADoNiS – the Karlsruhe Astrophysical Database of Nucleosynthesis in Stars, v.1.0,” University of Frankfurt, Frankfurt, Germany (2017), [Online] Available at <http://exp-astro.physik.uni-frankfurt.de/kadonis1.0/>.
- [27] F. Käppeler and R. Reifarh, “Activation data from karlsruhe revisited,” tech. rep. (2021). INDC International Nuclear Data Committee.
- [28] G. Walter, H. Beer, F. Käppeler, and R. D. Penzhorn, “The s-process branching at Kr-85,” *ASTRON. ASTROPHYS.* **155**, 247 (1986).
- [29] N. Fotiades, M. Devlin, R. O. Nelson, and T. Granier, “Low-spin states in ^{86}Kr from the (n, n') reaction,” *PHYS. REV. C* **87**, 044336 (2013).
- [30] A. J. Koning and J. P. Delaroche, “Local and global nucleon optical models from 1 keV to 200 MeV,” *NUCL. PHYS. A* **713**, 231 (2003).
- [31] R. Capote, M. Herman, P. Obložinský, *et al.*, “RIPL – reference input parameter library for calculation of nuclear reactions and nuclear data evaluations,” *NUCL. DATA SHEETS* **110**, 3107 (2009).
- [32] G. P. A. Nobre, D. A. Brown, M. W. Herman, and A. Golas, “Constraining level densities through quantitative correlations with cross-section data,” *PHYS. REV. C* **101**, 034608 (2020).
- [33] G. P. A. Nobre, M. T. Pigni, D. A. Brown, *et al.*, “Newly evaluated neutron reaction data on chromium isotopes,” *NUCL. DATA SHEETS* **173**, 1 (2021).
- [34] J. J. Griffin, “Statistical model of intermediate structure,” *PHYS. REV. LETT.* **17**, 478 (1966).
- [35] J. M. Akkermans, H. Gruppelaar, and G. Reffo, “Angular distributions in a unified model of preequilibrium and equilibrium neutron emission,” *PHYS. REV. C* **22**, 73 (1980).
- [36] V. A. Plujko, “A new closed-form thermodynamic approach for radiative strength functions,” *ACTA PHYS. POLONICA B* **31**, 435 (2000).
- [37] J. M. Blatt and L. C. Biedenharn, “The angular distribution of scattering and reaction cross sections,” *REV. MOD. PHYS.* **24**, 258 (1952).
- [38] S. Raman, C. W. Nestor, and P. Tikkanen, “Transition probability from the ground to the first-excited 2+ state of even-even nuclides,” *AT. DATA NUCL. DATA TABLES* **78**, 1 (2001).
- [39] G. P. A. Nobre, A. Palumbo, M. Herman, D. Brown, S. Hoblit, and F. S. Dietrich, “Derivation of an optical potential for statically deformed rare-earth nuclei from a global spherical potential,” *PHYS. REV. C* **91**, 024618 (2015).
- [40] V. Avrigeanu, P. E. Hodgson, and M. Avrigeanu, “Global optical potentials for emitted alpha particles,” *PHYS. REV. C* **49**, 2136 (1994).
- [41] H. An and C. Cai, “Global deuteron optical model potential for the energy range up to 183 MeV,” *PHYS. REV. C* **73**, 054605 (2006).
- [42] F. D. Becchetti and G. W. Greenlees, “Nucleon-Nucleus Optical-Model Parameters, $A < 40$, $E > 50$ MeV,” *PHYS. REV.* **182**, 1190 (1969).

- [43] N. Otuka, E. Dupont, V. Semkova, *et al.*, “Towards a More Complete and Accurate Experimental Nuclear Reaction Data Library (EXFOR): International Collaboration Between Nuclear Reaction Data Centres (NRDC),” *NUCL. DATA SHEETS* **120**, 272 (2014).
- [44] V. Zerkin and B. Pritychenko, “The experimental nuclear reaction data (EXFOR): Extended computer database and Web retrieval system,” *NUCL. INST. METH. PHYS. RES. SECT. A: ACCEL. SPECTROMETERS, DETECT. ASSOC. EQUIP.* **888**, 31 (2018).
- [45] T. Kawano and K. Shibata, “Covariance evaluation system,” JAERI data/code, Japan Atomic Energy Research Institute, Tokai, Japan (1997).
- [46] A. Negret and B. Singh, “Nuclear Data Sheets for $A = 86$,” *NUCL. DATA SHEETS* **124**, 1 (2015).
- [47] “Evaluated Nuclear Structure Data File.” National Nuclear Data Center, Brookhaven National Laboratory.
- [48] W. Urban, K. Sieja, T. Materna, *et al.*, “Low-spin structure of $^{86}_{35}\text{Br}_{51}$ and $^{86}_{36}\text{Kr}_{50}$ nuclei: The role of the $g_{7/2}$ neutron orbital,” *PHYS. REV. C* **94**, 044328 (2016).
- [49] M. Martin, “Reduced gamma-ray matrix elements, transition probabilities and single-particle estimates.” [Memorandum] Oak Ridge, Tennessee: Oak Ridge National Laboratory (September 27, 1982).
- [50] National Nuclear Data Center, information extracted from the NuDat 2 database. <https://www.nndc.bnl.gov/nudat2/>.
- [51] E. Kondaiiah, N. Ranakumar, and R. Fink, “Neutron activation cross sections at 14.4 MeV for Kr and Xe isotopes,” *NUCL. PHYS. A* **120**, 337 (1968).
- [52] C. Kalbach and F. M. Mann, “Phenomenology of continuum angular distributions. I. Systematics and parametrization,” *PHYS. REV. C* **23**, 112 (1981).